Muñoz-Pina, S.; Ros-Lis, JV.; Argüelles Foix, AL.; Martínez-Máñez, R.; Andrés Grau, AM. (2020). Influence of the functionalisation of mesoporous silica material UVM-7 on polyphenol oxidase enzyme capture and enzymatic browning. Food Chemistry. 310:1-8. https://doi.org/10.1016/j.foodchem.2019.125741

INFLUENCE OF THE FUNCTIONALISATION OF MESOPOROUS SILICA MATERIAL UVM-7 ON POLYPHENOL OXIDASE ENZYME CAPTURE AND ENZYMATIC BROWNING

Sara Muñoz-Pina[1], José V. Ros-Lis[2,3]*, Ángel Argüelles[1], Ramón Martínez-Máñez[3,4], Ana Andrés[1]

[1] *Instituto Universitario de Ingeniería de Alimentos para el Desarrollo (IUIAD-UPV). Universitat Politècnica de València. Camino de Vera s/n, 46022, Valencia, Spain.*

[2] *Inorganic Chemistry Department, Universitat de València. 46100, Burjassot, Valencia Spain.*

[3] *CIBER de Bioingeniería, Biomateriales y Nanomedicina (CIBER-BBN)*

[4] *Instituto Interuniversitario de Investigación de Reconocimiento Molecular y Desarrollo Tecnológico. Universitat Politècnica de València - Universitat de València. Camino de Vera s/n, 46022, Valencia, Spain.*

*Corresponding author. Email: J.Vicente.Ros@uv.es

ABSTRACT

Polyphenol oxidase (PPO), also known as tyrosinase and catechol oxidase, is the enzyme responsible for enzymatic browning in foods. It causes undesirable organoleptic, nutritional and colour changes. Here, we report the preparation of five nanomaterials and a study of their ability to modulate PPO enzyme activity. The materials consist of UVM-7 supports (a mesoporous silica material) modified with diverse functional groups (i.e. amine, carboxylic acid, isocyanate, alkane and pyridine). We also studied the PPO immobilisation capability of the materials. All the materials, except the carboxylic acid functionalised one, offer high PPO loading capabilities and the immobilisation speed increases with functionalisation. Nevertheless, only a minor effect of the inhibition of

enzymatic browning was produced. Furthermore, the amine containing material was able to capture not only PPO, but also the oxidation products. Such behaviour was validated with fresh apple juice in which browning was avoided, even 90 minutes in the presence of oxygen at room temperature.

Key words: PPO; tyrosinase; inhibition; UVM-7; amines; apple juice

1. Introduction

The polyphenol oxidase (PPO) enzyme, also known as tyrosinase (monophenolase activity EC 1.14.18.1 and diphenolase activity EC 1.10.3.1), is a relevant type 3 copper protein responsible for catalysing the O-hydroxylation of monophenols and converting them into O-diphenols and, subsequently, catalysing the oxidation of O-diphenols to produce O-quinones (Kanteev, Goldfeder, & Fishman, 2015). These *ortho*-quinones are particularly reactive and their polymerisation produces different coloured pigments (e.g. black, brown, or even red), which, in turn, cause enzymatic browning. Polyphenol oxidase was first discovered in the mushroom by Schoenbein in 1856. Since then, it has been subject to numerous studies (Mayer, 2006). Some of the main topics approached in those works are: PPO characterisation (Decker, Schweikardt, & Tuczek, 2006), medical interest (Nakamura, Torikai, & Ohigashi, 2001), sensors (Reza, Ali, Srivastava, Agrawal, & Biradar, 2015), wastewater regeneration (Ba et al., 2018) or protein cross-linking and immobilisation (D.-M. Liu, Chen, & Shi, 2018b).

In food technology (Mishra, Gautam, & Sharma, 2013), PPO is present in a wide variety of foods. Polyphenol oxidase can be one of the causes, for example, of changes in colour when fruit flesh and juice come into contact with oxygen. Enzyme mediated colour change is known as enzymatic browning and causes significant modifications in

organoleptic, nutritional and colour properties, mostly in those foods with high percentages of tyrosinase and polyphenols.

Even though this reaction in some foods, like chocolate or tea, is essential and desirable (Macedo, Rocha, Ribeiro, Soares, & Bispo, 2016), browning is undesirable in fruits or vegetable that have notable amounts of polyphenols. As consumers' acceptability of products depends mostly on colour and appearance, enzymatic browning has become a crucial target for food processing and, therefore, for the food industry.

Among the available techniques to prevent or avoid the enzymatic browning reaction, pasteurisation is the most widely used industrial method because it can inactivate enzymes and destroy microorganisms simultaneously. Although pasteurisation guarantees the safety and shelf life of fruits and vegetables, application of high temperatures (between 60-90°C) may destroy some thermosensitive nutrients that are very common in these food matrices, such as vitamins, carotenoids and anthocyanins (Buckow, Kastell, Terefe, & Versteeg, 2010).

To avoid the negative effects of pasteurisation, the food industry has developed alternative methods to inactivate PPO, including high pressure (Kaushik, Rao, & Mishra, 2016), supercritical carbon dioxide (Y. Liu, Hu, Zhao, & Song, 2012), ultrasound (Bhat & Ming Goh, 2017), gamma irradiation (Kim, Song, Lim, Yun, & Chung, 2007) and adding certain chemical agents, such as acidulants (Jiang, Kim, Nam, Yim, & Eun, 2016). Nonetheless, some of these techniques have not been completely transferred to the industry given their high cost and, in some cases, their major machinery requirements. Only the addition of some chemical agents, such as sulphites or acids that lower pH, has been widely used as an alternative to pasteurisation. Even though sulphites are powerful inhibitors of PPO, their use as food additives is not recommended because these

compounds might cause allergenic reactions. In this scenario, research that has focused on finding new methodologies capable of inhibiting enzymatic browning without altering food quality is a relevant field.

From another point of view, nanotechnology has enabled much progress to be made in many fields, such as biomedicine (Giner-Casares, Henriksen-Lacey, Coronado-Puchau, & Liz-Marzán, 2016), chemical sensors (Pallás, Marcos, Martínez-Máñez, & Ros-Lis, 2017), etc. The food technology sector is no stranger to this revolution and has also shown an interest in finding nanotechnological solutions for a number of applications (Poyatos-Racionero, Ros-Lis, Vivancos, & Martínez-Máñez, 2018). For instance, the interactions between nano-scale materials and proteins have been well studied (Shemetov, Nabiev, & Sukhanova, 2012) given the possibility of modulating enzyme activity or of modifying the enzyme structure and function (Chen, Zeng, Xu, Lai, & Tang, 2017). Although the use of nano-scale materials, such as nanoparticles, can be an interesting tool to stop enzymatic browning in industrial food processing, this has been rarely addressed to date. In this context, Corell Escuin et al. (2017) reported the ability of mesoporous silica materials to immobilise the PPO enzyme, where pore size and pH were the major factors that affected their immobilising capacity. Along the same line, Muñoz-Pina et al. (2018) studied the PPO inhibitory capacity of several thiol-functionalised mesoporous silica materials with different shapes and pore sizes. The UVM-7 material, a silica based MCM-41 type mesoporous material, which contains both mesopores and textural pores, has also been reported to be able to immobilise and inhibit polyphenol oxidase in both model and real systems (Muñoz-Pina et al., 2018).

Based on the hypotheses that the modification of the surface of the nanomaterials can influence the ability of the UVM-7 nanomaterials to immobilise PPO and to inhibit

97 enzymatic browning, the aim of this work is to evaluate the influence of the surface
98 coating in the modulation of the enzyme activity in model systems and the inhibition of
99 enzymatic browning in apple juice.

100 **2. Materials and Methods**

101 *2.1. Chemicals*

102 Tetraethyl orthosilicate (TEOS) reagent grade 98%, triethanolamine ($TEAH_3$) reagent
103 grade 98%, N- cetyltrimethylammonium bromide (CTABr) for molecular biology ≥99%,
104 3-aminopropyl triethoxysilane (APTES) ≥98%, trimethoxy(octadecyl)silane technical
105 grade 90% (GC), 3-triethoxysilyl propyl isocyanate 95%, 3-mercaptopropyl
106 trimethoxysilane 95%, 2,2'-dipyridyl disulphide 98%, acetic acid glacial ReagentPlus
107 ≥99%, mushroom tyrosinase lyophilized powder ≥1000 unit/mg solid, dopamine
108 hydrochloride were provided by Sigma-Aldrich (Sigma-Aldrich, USA) and used without
109 further purification. N-[(3-trimethoxysilyl) propyl]ethylenediamine triacetic acid
110 trisodium salt 40% in water was provided by Fluorochem (Fluorochem, UK). Sodium
111 dihydrogen phosphate anhydrous extra pure and di-sodium hydrogen phosphate
112 anhydrous extra pure were supplied by Scharlau (Sharlab S.L., Spain) and sodium acetate
113 anhydrous for analysis ACS by Panreac (Panreac AppliChem, Barcelona, Spain). The
114 mesoporous material UVM-7 was prepared following known procedures (Comes et al.,
115 2009). Following a modification of the so-called “atrane” route, a mixture of 0.05 mol of
116 TEOS and 0.17 mol of $TEAH_3$ was heated at 120°C until no condensation of ethanol was
117 observed in a Dean–Stark apparatus. Afterwards, the mixture was cooled down to 90°C
118 and 4.56 g of CTABr were added, followed by 80 mL of water. The mixture was aged at
119 room temperature for 24 h. The resulting precipitate was collected by centrifugation

and washed with water. Lastly, the solid was dried at 70°C and calcined at 550°C under static air atmosphere, as an oxidant atmosphere, for 5 h to remove the CTABr surfactant. Apples of the variety Golden Delicious were obtained from a local retailer and used to prepare juice.

2.2. Synthesis of the UVM-7 functionalised materials

Five materials were prepared with diverse functionalisations.

2.2.1 Synthesis of U-NH_2

One gram of calcined UVM-7 was treated with excess APTES (10 mmol) in 30 mL of acetonitrile (ACN). The suspension was allowed to react for 16 h at room temperature. Then the resultant solid was isolated by centrifugation, washed with ACN and finally dried at 37°C.

2.2.2 Synthesis of U-NCO

Solid U-NCO was prepared by allowing 1 g of calcined UVM-7 to come into contact with excess 3-(Triethoxysilyl) propyl isocyanate (10 mmol) in 30 mL of acetonitrile. The suspension was allowed to react for 16 h at room temperature. Then U-NCO was isolated by centrifugation, washed with ACN and finally dried at 37°C.

2.2.3 Synthesis of U-py

For the synthesis of U-py, 1 gram of UVM-7 was reacted with 10 mmol of (3-Mercaptopropyl) trimethoxysilane in 30 mL of acetonitrile for 16 h. After isolation by centrifugation, the solid was washed with ACN and dried at 37°C. Afterwards, 250 mg of the resultant solid were resuspended in 8.5 mL of ACN containing 2.5 mmol of 2,2'-Dipyridyl disulphide and aged for 12 h. Lastly, the solid was isolated by centrifugation and subsequent washing with ACN.

2.2.4 Synthesis of U-C_{18}

144 Solid U-C_{18} was obtained by reacting 10 mmol of trimethoxy(octadecyl)silane and 1 g of
145 UVM-7 in 30 mL of toluene. The mixture was reacted at room temperature for 16 h. The
146 resulting solid was washed with methanol and dried at 37°C.
147 *2.2.5 Synthesis of U-EDTA*
148 Solid U-EDTA was prepared by adding 10 mmol of 40%n-[(3-trimethoxysilyl) propyl]
149 ethylenediamine triacetic acid trisodium salt in water to 30 mL of a suspension of
150 methanol containing 1 g of UVM-7. Four drops of acetic acid glacial were poured and
151 the mix was aged for 16 h at room temperature. The solid was washed with water and
152 acetone and was dried at 37°C.
153 *2.3. Characterisation of the UVM-7 functionalised materials*
154 The characterisation of the UVM-7 functionalised materials was carried out by low-angle
155 X-ray powder diffraction (XRD), Bruker D8 Advance CuKα radiation), transmission
156 electron microscopy (TEM, JEOL–jem-1010), nitrogen adsorption/desorption isotherms
157 and thermogravimetric analysis (TGA) and FTIR spectroscopy was carried out with a
158 Bruker Tensor-27. Nitrogen adsorption/desorption isotherms were carried out in a
159 Micromeritics ASAP 2010 automated sorption analyser at the liquid nitrogen
160 temperature (-196°C.). Samples were degassed at 120°C in a vacuum overnight. The
161 specific surface area was determined by applying the BET model (Brunauer, Emmett, &
162 Teller, 1938) from the adsorption data within the low-pressure range. Pore size was
163 calculated following the Barret-Joyner-Halenda model (BJH) (Barrett, Joyner, & Halenda,
164 1951) . From the XRD analysis (Neimark, Ravikovitch, Grün, Schüth, & Unger, 1998), the
165 a_0 cell parameter and the wall thickness of the silica materials were calculated (see
166 Table1). A TGA was used to estimate the concentration of the different functionalised
167 chemical groups on the UVM-7 surface using an oxidant atmosphere (air, 80 mL/min)

with a heating programme (10°C/min from 393 to 1273 K and an isothermal heating step at this temperature for 30 min).

2.4. Oxygen consumption

The initial oxygen consumption rate was followed by an Oxyview System from Hansatech during the oxidation reaction of the dopamine using a Clark Type Oxygen electrode. For this assay, the different synthesised materials (UVM-7, U-NH_2, U-NCO, U-py, U-EDTA and U-C_{18}) were used at the 3 mg/mL ratio in phosphate buffer (10 mM, pH 5.5). Solutions were sonicated for 5 minutes to acquire the materials' correct dispersion. One millilitre of the solution was allowed to come into contact with 0.25 mL of the PPO solution of 375 U/mL in the reaction vessel to be stirred for 10 minutes. Afterwards, 0.25 mL of dopamine was added. Two different dopamine concentrations were tested: 0.16 mM and 2.5 mM. The initial reaction rate was obtained from the slope of the linear part of the oxygen consumption curve during the first minutes. A control with no material was also studied. Assays were done in triplicate at 25°C.

2.5. Colorimetric determination of PPO activity

In a typical experiment, 3 mg of material were suspended in 1 mL of phosphate or buffer 10 mM at a defined pH of 5.5. After sonication, 0.25 mL of a tyrosinase solution of 375 U/mL was added and the mixture was aged for 10 min by stirring. Subsequently, 0.25 mL of dopamine solution 0.16 mM or 2.5 mM was/were added and the enzymatic reaction was left for 1 h. Then the suspension was centrifuged, and the supernatant was measured by spectrophotometry (Thermo scientific Helios-zeta) at 420 nm using 2.5 mL plastic cuvettes. The assays done in the absence of material were also carried out as the control. To test the influence of the pH, the same protocol was followed using

phosphate-acetate 10 mM as buffer at pH 4.5, 5.5 and 6.5, to study the influence of pH. Assays were done in duplicate.

2.6. Material immobilisation capacity

The Bradford assay (Bradford, 1976) was performed to study the capability of UVM-7 and the UVM-7 functionalised materials to immobilise PPO. For this purpose, 0.25 mL of a tyrosinase solution of 375 U/mL was allowed to come into contact with 3 mg of the corresponding mesoporous material suspended in 1 mL of phosphate buffer at pH 5.5. The resulting suspension was stirred for two different times (10 and 120 minutes) and then centrifuged (9600 RCF, 3 min). From the supernatant, two 100-μL aliquots were taken to perform the Bradford assay. The amount of free enzyme in solution was obtained by interpolation in a calibration line, obtained using tyrosinase from mushroom. The immobilisation yield was calculated according to Eq. (1), where P_0 and P_i were the amounts of protein present in the solution in the presence and absence of the material, respectively, calculated from the calibration line. An ANOVA test was used to determine significant differences.

$$Immobilisation\ yield\ (\%) = \frac{P_0 - P_i}{P_0} * 100 \qquad (1)$$

From the rest of the supernatant, 900 μL were taken and allowed to come into contact with 180 μL of dopamine 15 mM to determine residual enzyme activity. Measurements were taken every 10 seconds at 420 nm. Assays were done in triplicate. Relative activity was calculated according to Eq. (2), where V_{o0} is the control initial rate and V_{oi} is the initial rate obtained for the different samples.

$$Relative\ activity\ (\%) = \left(\frac{V_{0i}}{V_{00}}\right) * 100 \qquad (2)$$

2.8. Material testing in apple juice

214 Apples of the cv. Golden Delicious variety were first washed and then liquefied in a
215 Moulinex centrifugal JU200045. A 2-mL aliquot of the freshly liquefied juice was taken
216 and mixed with two different amounts of U-NH_2 (20 mg and 3 mg). Simultaneously,
217 another 2-mL aliquot with no material was used as the control sample. These blends
218 were stirred at 400 rpm for 1 minute. Subsequently, the different samples were filtrated
219 under vacuum using Whatman filter paper grade 41 to eliminate the mesoporous
220 material. The new aliquots continued to be stirred and colour changes were followed by
221 image taking. In order to measure enzymatic browning, 200 µL of the filtered juice were
222 diluted in 1 mL of water and the colour change was followed by measuring the
223 absorbance at 420 nm in a Thermo scientific Helios-zeta. An ANOVA test was used to
224 determine significant differences.
225
226 **3. RESULTS AND DISCUSSION**
227 *3.1. Materials selection and characterisation*
228 We recently reported that calcined UVM-7 material can inhibit enzymatic browning
229 better than other silica-based mesoporous materials such as MCM-41 with nanometric
230 or micrometric particle size or aerosil (Corell Escuin et al., 2017). We also observed that
231 this browning inhibition can be modulated by the functionalisation of the silica surface.
232 Furthermore, silica materials functionalised with thiol groups can fully inhibit enzymatic
233 browning in apple juice (Muñoz-Pina et al., 2018). In order to gain further insight into
234 the enzymatic browning process and in an attempt to improve the use of the UVM-7
235 mesoporous support to immobilise and inhibit enzymatic browning, five materials were
236 herein prepared that consisted of UVM-7 supports functionalised with two different
237 amines (APTES and pyridine; materials U-NH_2 and U-py, respectively), carboxylic acid

238 (EDTA; material U-EDTA), an alkane (C_{18}; material U-C_{18}) and an isocyanate (material U-
239 NCO) (see Figure 1). These functional groups showed diverse charge, reactivity and
240 supramolecular binding properties. Propyl isocyanate was chosen for its ability to react
241 with different nucleophiles, including the amines and alcohols usually present in the
242 residues of proteins (Canilho et al., 2013). The functionalisation with amines or
243 carboxylic acids resulted in polar charged surfaces that can be modified with variations
244 in the pH of the solution. In this context, APTES has been widely used to immobilise
245 proteins (D.-M. Liu, Chen, & Shi, 2018a). The metal chelating properties of the amino
246 and carboxylate groups can result in the coordination, or eventually in the
247 demetallation, of the two copper active centres in PPO, with the consequent decrease
248 in the enzymatic activity. Also, the long chain alkane derivative (C_{18}) offers to study the
249 influence of a hydrophobic surface.
250 X-ray powder diffraction and TEM techniques were used to confirm the mesoporous
251 structure of the starting UVM-7 and the final functionalised materials. The XRD pattern
252 of the UVM-7 solid showed low-angle reflection, which is related to a hexagonal array
253 of pores indexed as a (100) Bragg reflection, and characteristic of UVM-7 materials. The
254 five surface-modified materials (U-NH_2, U-py, U-NCO, U-EDTA and U-C_{18}) maintained the
255 X-ray powder diffraction pattern observed for the calcined support (UVM-7), which
256 agrees with the maintenance of the mesoporous structure during the functionalisation
257 process (Figure S1). d_{100} spacing was calculated for all the materials using the data from
258 the X-ray powder diffraction experiments. As seen in Table 1, the d_{100} spacing values
259 were around 43 Å in all cases, which coincides with other reported values (Haskouri et
260 al., 2009). The hexagonal porous structure was also confirmed by TEM (Supplementary

261 Material, Figure S2). The TEM images also indicated that no substantial changes
262 occurred in the structure of the support after functionalisation.
263 The TGA (Supplementary Material, Figure S3) revealed that the amount of organic
264 content varied among the diverse materials. As seen in Table 1, the amount of organic
265 matter ranged from 0.16 to 2.95 mmol (g SiO_2)$^{-1}$ for U-NCO and U-NH_2, respectively,
266 which are similar values to those found for other reported UVM-7-functionalised
267 materials (Pallás et al., 2017). Although functionalisation did not modify the structure of
268 the support, it strongly impacted the specific surface area and porosity. The calcined
269 material (UVM-7) had a specific surface area that came close to 900 m^2 g^{-1}, which had a
270 bimodal porous system with pores of 2.7 nm (mesopores) and 40 nm (textural porosity).
271 The specific area slightly reduced due to the organic functionalisation for U-C_{18}, U-NCO
272 and U-py. However, the material with the highest number of moles of organic molecules
273 per gram of solid (U-NH_2) drastically dropped in the total specific area, with a value of
274 216 m^2g^{-1}. Even stronger is the blocking effect observed for U-EDTA (119 m^2g^{-1}), a
275 material with an organic content of only 0.97 mmol (g SiO_2)$^{-1}$). This behaviour can be
276 explained keeping in mind that while the organic residue in the U-NH_2 contains three
277 carbon and one nitrogen atoms, in the U-EDTA material the organic residue shows
278 eleven carbon, two nitrogen and four oxygen atoms, therefore a much bigger molecular
279 volume per molecule.
280 From Table 1, we can observe that this reduction in the specific area for both U-NH_2 and
281 U-EDTA was also accompanied by a reduction in the mesopore volume, while only minor
282 variations were noted for the textural pore volume. It seems that only those materials
283 loaded with the highest amount of organic groups (U-NH_2 and U-EDTA) were able to
284 block the little size mesopores with approximately 2.7 nm of diameter. However, they

285 cannot block to the same extent big size textural pores with a diameter close to 40 nm
286 (see Table 1). We must consider that the short length of the organic chains (up to 18
287 carbons) is not able long enough to block a pore with a radius close to 20 nm.

288 *3.2. Studies of PPO activity in the presence of the UVM-7 functionalised materials*

289 Enzymatic browning is a two-step process comprising first the PPO-mediated oxidation
290 of the substrate (typically phenols or catechols) to quinones by oxygen, followed by non-
291 enzymatic polymerisation that generates the final brown melanoid products. Thus, to
292 characterise the PPO enzymatic response in the presence of the functionalised UVM-7
293 materials, two sets of assays were carried out. Firstly, oxygen consumption due to the
294 PPO catalysed dopamine oxidation was determined by the Oxyview system and the main
295 kinetic parameters of the reaction were calculated from the initial reaction rate.
296 Secondly, the colour formed during the 1-hour reaction was measured as an approach
297 to see the effect of inhibition in the long term. Similar experiments were run with the
298 non-functionalised UVM-7 material. Moreover, measurements were taken in the
299 absence of nanomaterials and were included as a reference.

300 Figures 2a and 2b contain the enzymatic activity measured by the two methodologies.
301 The activity in the absence of material was used as a reference (100%). For the sake of
302 clarity, a dashed line was added to indicate this value. As seen in Figure 2a, the initial
303 oxygen consumption rate in the presence of the non-functionalised UVM-7 led to no
304 significant differences in the values observed in the absence of material (100%). This
305 indicates that the presence of UVM-7 does not interfere in the first enzymatic browning
306 stage when oxygen is consumed during polyphenols oxidation. The same behaviour was
307 observed for U-NCO. However, when PPO came into contact with U-C_{18} or U-EDTA, the
308 oxidation rate of dopamine dropped by 20-25% regardless of the amount of the

309 substrate present in the medium. On the contrary, U-py or U-NH_2 showed differences
310 with the substrate (i.e. dopamine) concentration. At high dopamine concentrations,
311 over the Michaelis constant (K_M), the initial reaction rate dropped by around 20%, but
312 the rate fell 50% for U-NH_2 and 30% for U-py at lower dopamine concentration. The
313 dependence of the rate inhibition on the substrate concentration found for U-NH_2 and
314 U-py, and the fact that inhibition was greater when the substrate concentration was
315 low, suggests a competitive inhibition mechanism. In this kind of mechanism, the
316 material and substrate would compete for access to the binuclear copper active centre
317 and the formation of the enzyme-substrate or the enzyme-inhibitor complex. In this kind
318 of systems, the increase in the substrate concentration displaces the inhibitor modifying
319 the relative activity. Otherwise, the inhibition rate would be the same, regardless of the
320 substrate concentration, as observed for U-C_{18}, for example. Furthermore, this
321 evidences that U-NH_2, in particular, can lower the initial rate of the PPO-mediated
322 oxidation reaction by slowing down the process, at least for short times.
323 In order to evaluate the enzymatic response for long times in the presence of
324 mesoporous materials, the enzymatic reaction between dopamine and PPO was allowed
325 to continue for 1 h and the absorbance at 420 nm measured after centrifugation (Figure
326 2b). Even though the initial conversion rate of polyphenols was delayed in some cases,
327 it would seem that enzymatic browning did not dramatically change after 1 h with any
328 of the studied materials. Once again, supports UVM-7, U-C_{18} and U-EDTA showed the
329 same response with both large and small amounts of substrate in the medium (about
330 85 %). In contrast, U-py and U-NH_2 responses were substrate-/concentration-
331 dependent.
332 *3.3. PPO immobilisation assays*

As noted above, the UVM-7 mesoporous material is characterised by having a bimodal porous system that renders material advantages for enzyme immobilisation compared to other mesoporous materials. By way of example, the well-known mesoporous silica MCM-41 has difficulties to immobilise large enzymes given its relatively small pore size (Yiu, Wright, & Botting, 2001b). In contrast, Tortajada et al. (2005) reported the ability of UVM-7 to load small enzymes into its mesopores, and also the ability to immobilise larger proteins in the textural pores between nanoparticles. These authors also showed a fast adsorption rate and high enzyme loading for bimodal UVM-7 silica. The advantage of this special topology of the UVM-7 material with PPO has also been demonstrated in calcined and thiol functionalised UVM-7 (Muñoz-Pina et al., 2018).

To better understand the mechanism of inhibition and to evaluate the capacity of the materials to immobilise PPO, the Bradford method was used to quantify the amount of protein that remained in the solution after coming into contact with the supports. Two contact times (10 and 120 minutes) between the enzyme and silica materials were evaluated.

Table 2 provides the results of the immobilisation tests. In general, all the functionalised materials (except for U-EDTA) offered immobilisation yields higher than 80%, even at times as short as 10 minutes. Thus, the materials show an interesting ability to capture the mushroom tyrosinase from the solution. The different behaviour noted for U-EDTA could be due to the high concentration of the carboxylic groups in the nanomaterial, which would endow the particle a negative charge under the given conditions. This charge could influence the interaction between the material and the enzyme, which would hinder adsorption.

356 It seems that the functionalisation could have a positive effect on the reduction of the
357 time necessary to immobilize the tyrosinase. For the non-functionalised UVM-7, the
358 immobilisation of PPO is slower than for the functionalised materials, with an
359 immobilization yield of 59 % at 10 minutes that reach 90% when the contact time was 2
360 h (see Table 2). No significant differences for $p<0.005$ were found in the immobilisation
361 yield between both contact times for the other materials. This implies that the
362 functionalisation of UVM-7 improves the speed of enzyme's immobilisation with values
363 over 80% for U-C18, U-NCO and U-py, which was complete (100%) for U-NH_2. This result
364 agrees with other authors who, for instance, achieved the almost complete
365 immobilisation of other enzymes using supports functionalised with amino groups as
366 anchors (Yiu, Wright, & Botting, 2001a; Zou et al., 2014).
367 Furthermore, we performed an experiment to verify if the solution had free enzyme and
368 it maintained its activity in solution after the exposition to the material. For this purpose,
369 tyrosinase was exposed to the material, followed by the material removal loaded with
370 the immobilized enzyme. The activity assay of the supernatant (900 μL) was tested by
371 adding 180 μL of dopamine 15 mM and measuring the initial activity rate
372 spectrophotometrically with the variation of absorbance at 420 nm. As seen in Table 2
373 (% relative activity columns), those materials with high immobilisation capabilities (i.e
374 U-NH_2, U-C_{18}, U-NCO and U-py) offered minimal residual enzyme activity in the
375 supernatant, which coincides with the results obtained in the immobilisation tests. For
376 the assay carried out with non-functionalised UVM-7, the supernatant showed certain
377 activity after at a 10-minute contact time, which confirms that this material needs longer
378 times to completely immobilise the enzyme. Furthermore, as expected from the
379 immobilisation yield, U-EDTA presented the most activity, but also a drop of about 35%

in relative activity compared to the sample that did not come into contact with the materials. This finding suggests that the material could induce certain enzyme inhibition, even if not immobilised.

As can be deduced from the data the materials offer a strong tendency to capture the tyrosinase, but the enzyme maintains a significant activity, even when it was immobilised on the UVM-7 functionalised materials. This is supported by the high immobilisation yields close to 90-100 % (see table 2) but a reduction in the oxygen consumption and absorbance at 420 nm (see Section 3.2) of only 20 to 50 %. Moreover, the confirmation of the activity of the enzyme on the material is supported by an inhibition around 99% for the supernatant after removing the material loaded with the enzyme for most of the materials.

3.4 Effect of pH on the material-PPO interaction.

Mesoporous material U-NH_2 showed the best PPO inhibitory properties and was the only support to slow down the initial oxygen consumption due to the oxidation of dopamine up to 50% at a low substrate concentration. Its immobilising power was the highest effective and fastest of all the studied materials. For this reason, this functionalised UVM-7 support (U-NH_2) was selected for further study the effect of pH on the nanomaterial-enzyme interaction. Three different pH values were evaluated using phosphate-acetate 10 mM buffer (4.5, 5.5 and 6.5) to explore the usual pH range in fruits and vegetables. Furthermore, U-C_{18}, a material lacking pH-sensitive groups, was also used for comparison purposes. Two concentrations of material were used (3 mg/mL, Figure 3a) or high (10 mg/mL, Figure 3b) to study the influence of the concentration of the material in the inhibition capability. In all the cases the material,

403 the enzyme and the substrate were put in contact together and the browning measured
404 in the supernatant after centrifugation.
405 The results are summarized in Figure 3. At a first glance, we can observe that the
406 material U-NH_2 offers a behaviour much more dependent on the pH than the alkyl
407 functionalised homologous U-C_{18}. As the pH basifies the absorbance at 420 nm in
408 solution decreases. It shows the same tendency at the two concentrations of material,
409 although the variation with the pH increases with the amount of material present.
410 As can be seen in Figure 3 and the picture inserted in Figure 3b, at pH 4.5 and after
411 centrifugation, the solution shows values of relative absorbance close to 100% and the
412 U-NH_2 material presents a white colour. This suggests that at pH 4.5 the U-NH_2 material
413 would offer a weakened tendency to immobilise the enzyme. The isoelectronic point of
414 PPO is sited around pH 5 (Fan & Flurkey, 2004) and, therefore at pH 4.5, a certain
415 repulsion between the PPO enzyme and the positive charges of protonated amino
416 groups was expected to preclude immobilisation. This effect would diminish at less
417 acidic pH.
418 At pH 6.5 the suspension containing 10 mg of U-NH_2/mL developed an intense dark
419 brown colour. However, upon centrifugation, a black precipitate and a slightly coloured
420 solution were obtained, which suggests that the brown molecules generated during
421 polymerisation remained adsorbed in the material. This behaviour can be observed also
422 in the system containing 3 mg of U-NH_2/mL although to a minor extension. This
423 unexpected phenomenon can be explained by the reaction that can take place between
424 the catechol and the primary amines in the support. In fact, Yang et al. (Yang, Saggiomo,
425 Velders, Cohen Stuart, & Kamperman, 2016) described that the crosslinking between o-
426 quinones and primary amines results in the formation of more than 60 compounds in

just a few minutes via Michael-type addition or Schiff-base reactions. These processes are both fast and complex and have been employed to synthesise polymers (Wu et al., 2011). Hence the o-quinones formed in our sample could react with the primary amine from U-NH_2 to form polymers that remain attached to particles by leaving the solution colourless when the material is removed. Therefore, the U-NH_2 immobilisation capability to immobilise the PPO enzyme was complemented with the ability of the anchored amines to react with the oxidized quinones to leave the solution colourless after centrifugation or filtration.

3.5 U-NH_2 performance in apple juice

The performance of U-NH_2 particles in apple juice was tested to estimate the enzymatic browning inhibition of this material in food samples. When the mesoporous particles coated with amino groups were stirred with the recently made liquefied apple juice (3 mg/mL), no differences could be seen by the naked eye, and the measured colour differences were not significant ($p > 0.05$). This indicates that U-NH_2 is unable to inhibit enzymatic browning in apple juice when the nanomaterial is added to the liquefied sample.

However, when considering the great immobilisation power of this material as explained above, another test was done by removing particles from the medium by vacuum filtration using Whatman filter paper grade 41 after 1 minute. The result (Figure 4A and 4B) revealed that, in the presence of 3 mg of U-NH_2, the colour generated by enzymatic browning (measured as the absorbance at 420 nm) diminished by more than 50% after 90 minutes compared with the control. Furthermore, when the amount of material was increased to 10 mg, no change in colour by the naked eye was observed in the filtered juice for the first 20 minutes and absorbance values went below 0.5. Only after 90

451 minutes was a light orange colour noted which corresponded to an absorbance of 0.8,
452 which was only 25% of the control after the same reaction time. The absence of
453 significant enzymatic browning after the filtering of the material reveals that particles
454 remove the enzyme from the juice by avoiding the oxidation and polymerisation of
455 substrates.
456
457 **4. CONCLUSIONS**
458 Five UVM-7-based materials with diverse functionalities (amine, carboxylic acid, alkane
459 and isocyanate) were prepared and their influence on the enzymatic browning process
460 was studied. Functionalisation strongly influenced the immobilisation of the enzyme.
461 The negatively charged surface generated by carboxylic acid induced a reduction of
462 immobilisation capability. On the contrary, the other functionalisations improved the
463 immobilisation of the enzyme, particularly with short contact times (10 minutes) by
464 reaching 100% enzyme immobilisation for the U-NH_2 material. However, despite the fast
465 and high loading capability, the enzyme immobilised on the material retained a certain
466 degree of activity. When the materials continued to be in contact with solutions, PPO
467 activity remained around 80% and only U-NH_2 offered inhibition that came close to 50%
468 in oxygen consumption at a low dopamine concentration (0.16 mM). So this material is
469 more suitable for tests done in food samples. When the material was removed from the
470 solution, before adding the substrate, full enzymatic browning inhibition was observed
471 for most of the materials, which agrees with the high PPO immobilisation yield. The
472 experiments performed in fresh apple juice with U-NH_2 revealed that the material
473 offered a suitable approach to inhibit enzymatic browning if the material came into
474 contact with the liquefied apple juice when it was prepared and removed 1 minute later.

Hence these materials can be used to immobilise and remove PPO from juices and to avoid the enzymatic browning process. In particular, the amine-containing material is well-suited for such purpose as it seems able to capture not only the enzyme, but also products from oxidation.

AKCNOWLEDGMENTS

The authors are grateful to the Spanish Government (Projects RTI2018-100910-B-C44 and MAT2015-64139-C4-1) and the Generalitat Valencia (Project PROMETEO/2018/024) for support.

REFERENCES

Ba, S., Haroune, L., Soumano, L., Bellenger, J.-P., Jones, J. P., & Cabana, H. (2018). A hybrid bioreactor based on insolubilized tyrosinase and laccase catalysis and microfiltration membrane remove pharmaceuticals from wastewater. *Chemosphere*, *201*, 749–755.

Barrett, E. P., Joyner, L. G., & Halenda, P. P. (1951). The Determination of Pore Volume and Area Distributions in Porous Substances. I. Computations from Nitrogen Isotherms. *Journal of the American Chemical Society*, *73*(1), 373–380.

Bhat, R., & Ming Goh, K. (2017). Sonication treatment convalesce the overall quality of hand-pressed strawberry juice. *Food Chemistry*, *215*, 470–476.

Bradford, M. M. (1976). A rapid and sensitive method for the quantitation of microgram quantities of protein utilizing the principle of protein-dye binding. *Analytical Biochemistry*, *72*(1), 248–254.

Brunauer, S., Emmett, P. H., & Teller, E. (1938). Adsorption of Gases in Multimolecular Layers. *Journal of the American Chemical Society*, *60*(2), 309–319.

Buckow, R., Kastell, A., Terefe, N. S., & Versteeg, C. (2010). Pressure and Temperature Effects on Degradation Kinetics and Storage Stability of Total Anthocyanins in Blueberry Juice. *Journal of Agricultural and Food Chemistry*, *58*(18), 10076–10084.

Canilho, N., Jacoby, J., Pasc, A., Carteret, C., Dupire, F., Stébé, M. J., & Blin, J. L. (2013). Isocyanate-mediated covalent immobilization of Mucor miehei lipase onto SBA-15 for transesterification reaction. *Colloids and Surfaces B: Biointerfaces*, *112*, 139–145.

Chen, M., Zeng, G., Xu, P., Lai, C., & Tang, L. (2017). How Do Enzymes "Meet" Nanoparticles and Nanomaterials? *Trends in Biochemical Sciences*, *42*, 914–930.

Comes, M., Aznar , E., Moragues, M., Marcos, M. D., Martínez-Máñez, R., Sancenón, F., … Amorós, P. (2009). Mesoporous Hybrid Materials Containing Nanoscopic "Binding Pockets" for Colorimetric Anion Signaling in Water by using Displacement Assays. *Chemistry - A European Journal*, *15*(36), 9024–9033.

Corell Escuin, P., García-Bennett, A., Vicente Ros-Lis, J., Argüelles Foix, A., & Andrés, A. (2017). Application of mesoporous silica materials for the immobilization of polyphenol oxidase. *Food Chemistry*, *217*, 360–363.

Decker, H., Schweikardt, T., & Tuczek, F. (2006). The First Crystal Structure of Tyrosinase: All Questions Answered? *Angewandte Chemie International Edition*, *45*(28), 4546–4550.

Fan, Y., & Flurkey, W. H. (2004). Purification and characterization of tyrosinase from gill tissue of Portabella mushrooms. *Phytochemistry*, *65*(6), 671–678.

Giner-Casares, J. J., Henriksen-Lacey, M., Coronado-Puchau, M., & Liz-Marzán, L. M. (2016). Inorganic nanoparticles for biomedicine: where materials scientists meet medical research. *Materials Today*, *19*(1), 19–28.

Haskouri, J. El, Dallali, L., Fernández, L., Garro, N., Jaziri, S., Latorre, J., … Amorós, P. (2009). ZnO nanoparticles embedded in UVM-7-like mesoporous silica materials: Synthesis and characterization. *Physica E: Low-Dimensional Systems and Nanostructures*, *42*(1), 25–31.

Jiang, G.-H., Kim, Y.-M., Nam, S.-H., Yim, S.-H., & Eun, J.-B. (2016). Enzymatic browning inhibition and antioxidant activity of pear juice from a new cultivar of asian pear (Pyrus pyrifolia Nakai cv. Sinhwa) with different concentrations of ascorbic acid. *Food Science and Biotechnology*, *25*(1), 153–158.

Kanteev, M., Goldfeder, M., & Fishman, A. (2015). Structure-function correlations in tyrosinases. *Protein Science : A Publication of the Protein Society*, *24*(9), 1360–9.

Kaushik, N., Rao, P. S., & Mishra, H. N. (2016). Process optimization for thermal-assisted high pressure processing of mango (Mangifera indica L.) pulp using response surface methodology. *LWT - Food Science and Technology*, *69*, 372–381.

Kim, D., Song, H., Lim, S., Yun, H., & Chung, J. (2007). Effects of gamma irradiation on the radiation-resistant bacteria and polyphenol oxidase activity in fresh kale juice. *Radiation Physics and Chemistry*, *76*, 1213–1217.

Liu, D.-M., Chen, J., & Shi, Y.-P. (2018a). Advances on methods and easy separated support materials for enzymes immobilization. *TrAC Trends in Analytical Chemistry*, *102*, 332–342.

Liu, D.-M., Chen, J., & Shi, Y.-P. (2018b). Tyrosinase immobilization on aminated magnetic nanoparticles by physical adsorption combined with covalent crosslinking with improved catalytic activity, reusability and storage stability. *Analytica Chimica Acta*, *1006*, 90–98.

Liu, Y., Hu, X., Zhao, X., & Song, H. (2012). Combined effect of high pressure carbon dioxide and mild heat treatment on overall quality parameters of watermelon juice. *Innovative Food Science and Emerging Technologies*, *13*, 112–119.

Macedo, A. S. L., Rocha, F. de S., Ribeiro, M. da S., Soares, S. E., & Bispo, E. da S. (2016). Characterization of polyphenol oxidase in two cocoa (Theobroma cacao L.) cultivars produced in the south of Bahia, Brazil. *Food Science and Technology*, *36*(1), 56–63.

Mayer, A. M. (2006). Polyphenol oxidases in plants and fungi: Going places? A review. *Phytochemistry*, *67*(21), 2318–2331. https://doi.org/10.1016/J.PHYTOCHEM.2006.08.006

Mishra, B. B., Gautam, S., & Sharma, A. (2013). Free phenolics and polyphenol oxidase (PPO): The factors affecting post-cut browning in eggplant (Solanum melongena). *Food Chemistry*, *139*(1–4), 105–114.

Muñoz-Pina, S., Ros-Lis, J. V., Argüelles, Á., Coll, C., Martínez-Máñez, R., & Andrés, A. (2018). Full inhibition of enzymatic browning in the presence of thiol-functionalised silica

553 nanomaterial. *Food Chemistry*, *241*, 199–205.

554 Nakamura, Y., Torikai, K., & Ohigashi, H. (2001). A catechol antioxidant protocatechuic acid
555 potentiates inflammatory leukocyte-derived oxidative stress in mouse skin via a
556 tyrosinase bioactivation pathway. *Free Radical Biology and Medicine*, *30*(9), 967–978.

557 Neimark, A. V, Ravikovitch, P. I., Grün, M., Schüth, F., & Unger, K. K. (1998). Pore Size Analysis
558 of MCM-41 Type Adsorbents by Means of Nitrogen and Argon Adsorption. *Journal of*
559 *Colloid and Interface Science*, *207*(1), 159–169.

560 Pallás, I., Marcos, M., Martínez-Máñez, R., & Ros-Lis, J. (2017). Development of a Textile
561 Nanocomposite as Naked Eye Indicator of the Exposition to Strong Acids. *Sensors*, *17*(9),
562 2134.

563 Poyatos-Racionero, E., Ros-Lis, J. V., Vivancos, J.-L., & Martínez-Máñez, R. (2018). Recent
564 advances on intelligent packaging as tools to reduce food waste. *Journal of Cleaner*
565 *Production*, *172*, 3398–3409.

566 Reza, K. K., Ali, M. A., Srivastava, S., Agrawal, V. V., & Biradar, A. M. (2015). Tyrosinase
567 conjugated reduced graphene oxide based biointerface for bisphenol A sensor.
568 *Biosensors and Bioelectronics*, *74*, 644–651.

569 Shemetov, A. A., Nabiev, I., & Sukhanova, A. (2012). Molecular Interaction of Proteins and
570 Peptides with Nanoparticles, *6*(6), 4585–4602.

571 Tortajada, M., Ramón, D., Beltrán, D., & Amorós, P. (2005). Hierarchical bimodal porous silicas
572 and organosilicas for enzyme immobilization. *Journal of Materials Chemistry*, *15*(35–36),
573 3859.

574 Wu, J., Zhang, L., Wang, Y., Long, Y., Gao, H., Zhang, X., … Xu, J. (2011). Mussel-Inspired
575 Chemistry for Robust and Surface-Modifiable Multilayer Films. *Langmuir*, *27*(22), 13684–
576 13691.

577 Yang, J., Saggiomo, V., Velders, A. H., Cohen Stuart, M. A., & Kamperman, M. (2016). Reaction
578 Pathways in Catechol/Primary Amine Mixtures: A Window on Crosslinking Chemistry.
579 *PLOS ONE*, *11*(12), e0166490.

580 Yiu, H. H. ., Wright, P. A., & Botting, N. P. (2001a). Enzyme immobilisation using SBA-15
581 mesoporous molecular sieves with functionalised surfaces. *Journal of Molecular Catalysis*
582 *B: Enzymatic*, *15*(1), 81–92.

583 Yiu, H. H. P., Wright, P. A., & Botting, N. P. (2001b). Enzyme immobilisation using siliceous
584 mesoporous molecular sieves. *Microporous and Mesoporous Materials*, *44–45*, 763–768.

585 Zou, B., Hu, Y., Cui, F., Jiang, L., Yu, D., & Huang, H. (2014). Effect of surface modification of low
586 cost mesoporous SiO2 carriers on the properties of immobilized lipase. *Journal of Colloid*
587 *and Interface Science*, *417*, 210–216.

588

589

590 **TABLE CAPTIONS**

591 Table 1: Textural properties and organic content of the UVM-7 silica matrix as-made, calcined

592 and functionalised.

593 Table 2: Percentage of the immobilisation of enzymatic activity and the residual activity of the

594 enzyme in the supernatant.

595

FIGURE CAPTIONS

Figure 1: Illustration of the functional groups attached to the UVM-7 support and tested against the PPO enzyme

Figure 2: PPO enzymatic response (93.75U) in the presence of 3 mg of functionalised and non-functionalised UVM-7 in the presence of two different substrate concentrations (a) Initial oxygen consumption speed. (b) Colour formed after a 1-hour reaction between PPO and dopamine in the presence of the different materials.

Figure 3: Colour formed after a 1-hour reaction between 93.75U of PPO and 0.16mM of dopamine in the presence of the different materials and after centrifugation. (a) [material]= 3mg Material: (■) U-NH_2, and (▲) U-C_{18} (b) [material]= 10mg. Material: (■) U-NH_2, and (▲) U-C_{18}

Figure 4: A) Colour evolution in the Golden delicious apple juice filtered, followed by images. (a) 3 mg of U-NH_2/mL juice. (b) 10 mg of U-NH_2/mL juice. B) Colour difference of the filtered apple juice over time, and previously treated with 3 mg of U-NH_2/mL juice and 10 mg of U-NH_2/mL juice *versus* the control measured spectrophotometrically.

610 **Table 1**

Material	Area [a] (m^2g^{-1})	Mesopore volume[b] (cm^3g^{-1})	Mesopore diameter[b] (nm)	Textural pore diameter[b] (nm)	Textural pore volume[b] (cm^3g^{-1})	mmol /g SiO_2	d_{100}[c](Å)	2θ[d]([0])	a_0[e] (Å)	dw[f](Å)
UVM-7 As made	-	-	-	-	-	-	44.8	1.97	51.7	-
UVM-7 calcined	909.4	0.72	2.71	39.6	0.96	-	43.9	2.01	50.7	23.6
U-NH_2	251.6	0.15	2.62	37.5	0.62	2.95	44.8	1.97	51.7	25.5
U-C_{18}	819.7	0.64	2.65	35.3	0.79	0.16	43.9	2.01	50.7	24.2
U-NCO	831.2	0.56	2.47	34.3	0.69	0.85	42.3	2.09	48.8	24.1
U-py	835.6	0.63	2.57	31.4	0.67	0.29	42.3	0.13	48.8	23.1
U-EDTA	118.5	0.07	2.74	36.0	0.36	0.97	43.1	0.93	49.8	22.3

611 [a] BET specific surface calculated from the N^2 adsorption-desorption isotherms.
612 [b] Pore volumes and pore size (diameter) calculated from the N^2 adsorption-desorption isotherms.
613 [C] Diffraction peak of the reticular plane 100 calculated by $2d_{100}\,sen\theta=n\lambda$
614 [d] Angle of incidence for the reflection plane
615 [e] The cell parameter calculated by $a_0=2d_{100}*(\sqrt{3})^{-1}$
616 [f] Wall thickness was calculated by $dw= a_0 - d_p$, where d_p is the pore diameter.
617
618

Table 2.

Material	Immobilisation yield (%)		Relative activity (%)[a]	
	10 min	2 h	10 min	2 h
UVM-7	59 ± 6	92 ± 10	5.9 ± 1.4	1.52 ± 0.16
U-NH_2	100 ± 2	104 ± 8	0.4 ± 0.05	0.40 ± 0.10
U-C_{18}	90 ± 10	90 ± 4	0.07 ± 0.05	0.09 ± 0.05
U-NCO	88 ± 3	88 ± 6	1.1 ± 0.2	0.47 ± 0.09
U-py	80 ± 10	104 ± 18	0.31 ± 0.06	0.25 ± 0.05
U-EDTA	-	-	63 ± 3	70.0 ± 1.6

[a] Activity measured in the supernatant after the removal of the material loaded with the immobilised enzyme.

623

624 **Figure 1**

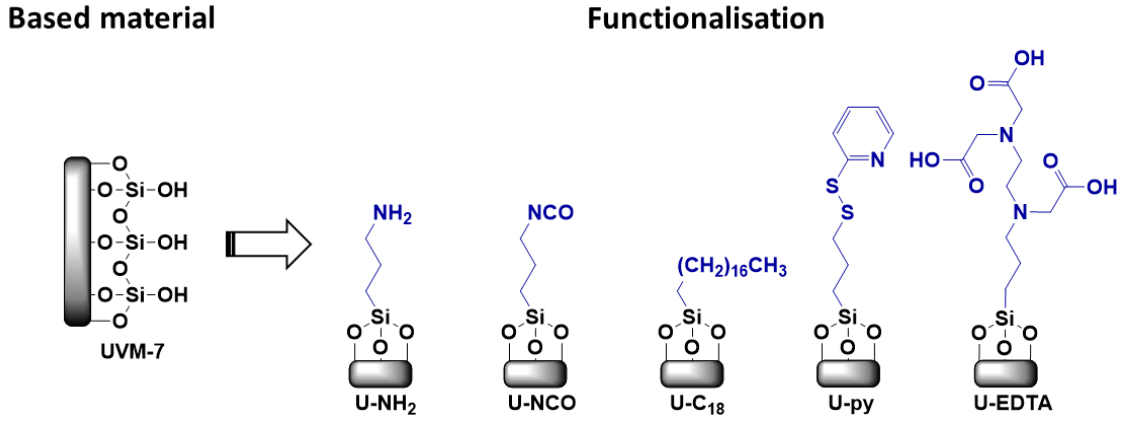

625

626 **Figure 2**

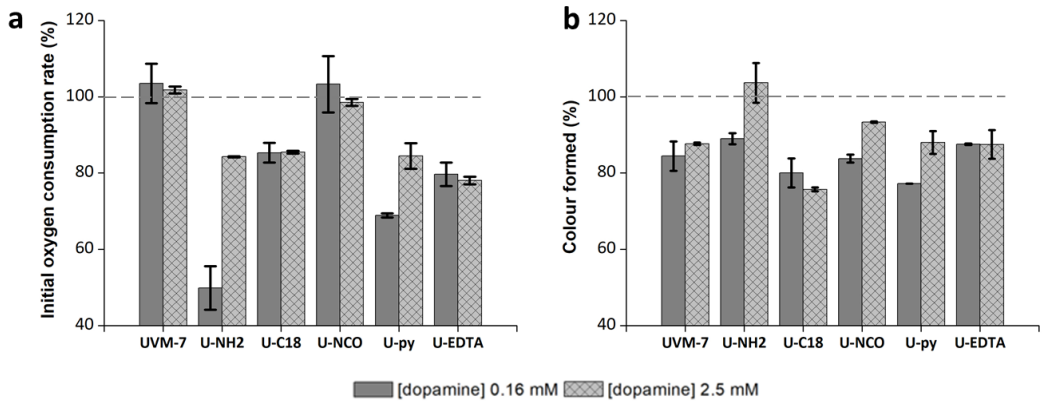

627

628 **Figure 3**

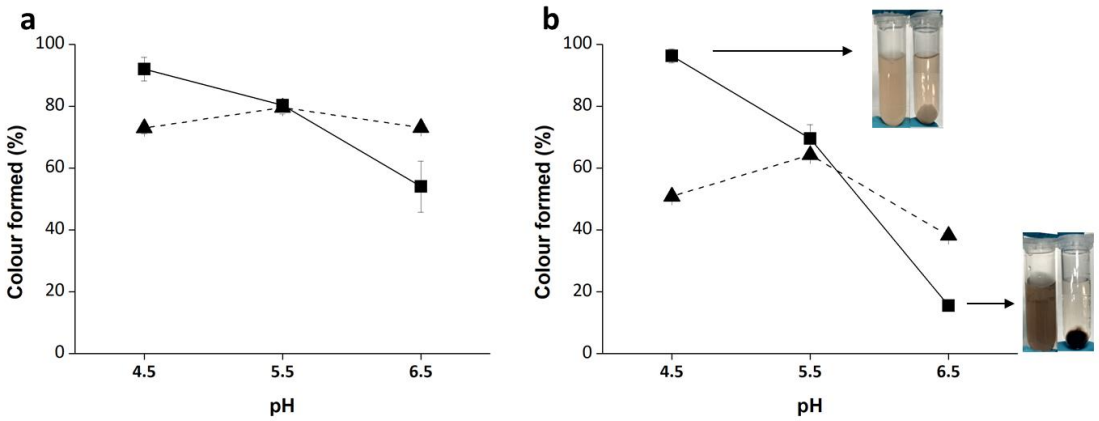

629

630

631 **Figure 4**

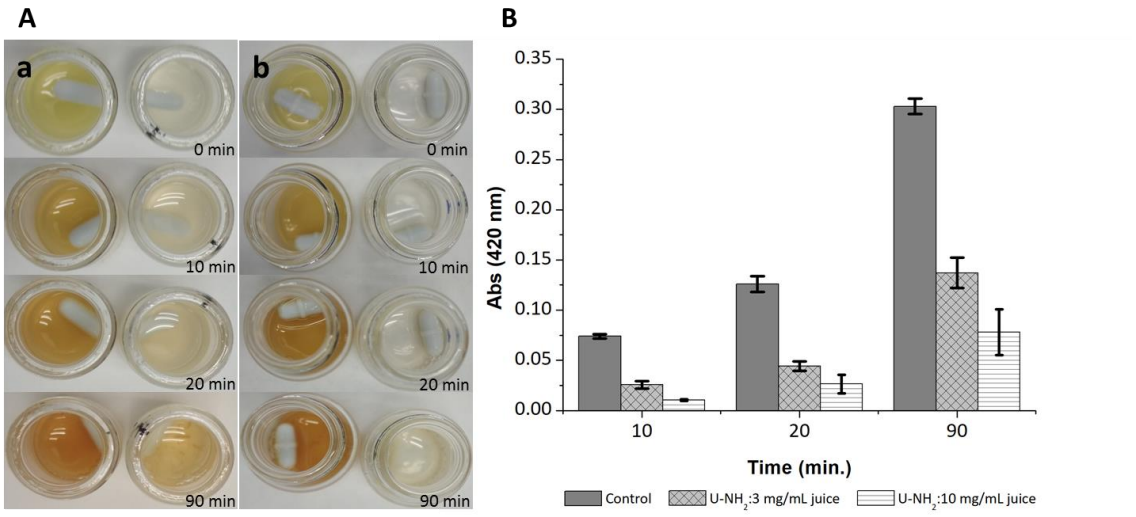

632